Nanoscale

Accepted Manuscript

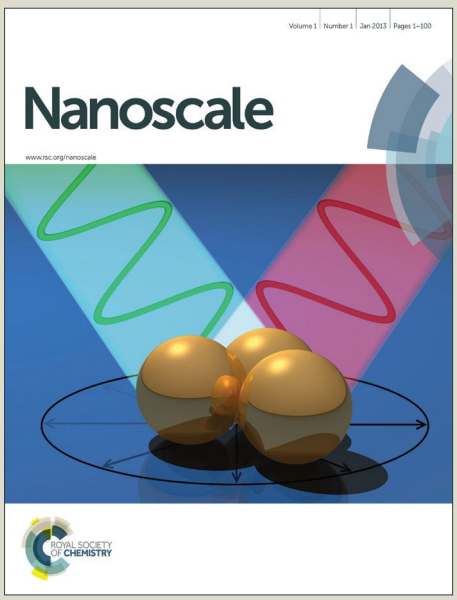

ROYAL SOCIETY OF CHEMISTRY

www.rsc.org/nanoscale

Nanoscale

RSCPublishing

ARTICLE

High Performance P(VDF-TrFE) Nanogenerator with Self-Connected and Vertically Integrated Fibers by Patterned EHD Pulling

Cite this: DOI: 10.1039/xoxx00000x

Received ooth January 2015,
Accepted ooth January 2015

DOI: 10.1039/xoxx00000x

www.rsc.org/

Xiaoliang Chen,[a]† Hongmiao Tian,[a]† Xiangming Li,[a] Jinyou Shao,*[a] Yucheng Ding,[a] Ningli An[b] and Yaopei Zhou[a]

Piezoelectricity based energy harvesting from mechanical vibrations have attracted extensive attention for its potential application in powering wireless mobile electronics recently. Here, a patterned electrohydrodynamic(EHD) pulling technology was proposed to fabricate a new self-connected, piezoelectric fiber array vertically integrated P(VDF-TrFE) nanogenerator, with a molecular poling orientation fully aligned to the principal excitation for maximized conversion and a well-bridged electrode pair for efficient charge collection. The nanogenerator is fabricated in a novel way by applying a voltage across an electrode pair sandwiching an air gap and an array of shallow micropillars, during which the EHD force tends to pull the micropillars upward, generating a microfiber array finally in robust contact with the upper electrode. Such a thermoplastic and EHD deformation of the microfibers, featured simultaneously by an electric field and by a microfiber elongation dominantly vertical to the electrode, leads to a poling orientation of P(VDF-TrFE) well coincident with the principal strain for the generator excited normal to the electrodes. The as-prepared piezoelectric device exhibits an enhanced output voltage up to 4.0V and current of 2.6μA, of which the piezoelectric voltage enhanced to be 5.4 times that from bulk film. Under periodic mechanical impact, electric signals are repeatedly generated from the device and used to power a seven-segment indicator, RBGY colored light-emitting diodes, and a large-scale liquid crystal display screen. These results not only provide a tool for fabricating 3D piezoelectric polymers but offer a new type of self-connected nanogenerator for the next generation of self-powered electronics.

Introduction

Harvesting clean and renewable energy directly from our living environment has been considered an attractive alternative to traditional rechargeable batteries for powering a variety of portable, wireless, micro-size or bio-implantable electronic devices.[1-3]. Since an early report on use of piezoelectric ZnO nanowires for electrical generation in 2006,[4] considerable attention has been focused on exploiting piezoelectric nano- or microstructures in various forms for capturing ambient mechanical vibrations and converting them into electricity to power small electronic devices.[5,6] So far, energy harvesters built by using a number of piezoelectric materials, including polyvinylidene fluoride (PVDF),[7,8] PZT,[3,9,10] ZnO,[11,12] PMN–PT,[13,14] BaTiO3,[15,16] etc., have been developed, demonstrating their concept applicability in self-powered small systems for sensing,[11,17] environmental monitoring,[7,18] and personal electronics.[16,19]

In comparison with inorganic piezoelectric materials, polymer based piezoelectric materials such as the PVDF or its copolymer P(VDF-TrFE), have a number of unique advantages, such as mechanical flexibility, ease to shape, chemical stability, and biocompatibility.[8,20] A variety of strategies have been proposed for fabricating polymeric piezoelectric power generators.[21-26] For example, Cha[21] and Wang[22] created nanoporous PVDF films using ZnO nanowires and ZnO nanoparticles, respectively, in a cast-etching process, showing an effective conversion of mechanical oscillations to electricity. For achieving an adequate energy conversion, these porous PVDF structures required a subsequent electrical poling to orient the molecular dipoles along the direction normal to the planar film. Recently, electrospinning processes based on electrohydrodynamic deformation have been presented to produce piezoelectric PVDF nanofibers, where the drawing force and electric field were considered to be able to naturally lead to a partial poling preferentially along the length of the nanofibers. To take a step further, Huang and Yin *et al.* present a kinetically controlled mechanoelectrospinning (MES)[27,28] to direct-write PVDF nanofibers onto a prestrained PDMS substrate, which has superior advantages for fabricating high flexible and stretchable piezoelectric devices used for

[a]State Key Laboratory for Manufacturing Systems Engineering, Xi'an Jiaotong University, Xi'an, Shaanxi 710049,China.
Corresponding author: jyshao@mail.xjtu.edu.cn (Jinyou Shao).
[b]College of Printing and Packaging Engineering, Xi'an University of Technology, Xi'an, Shaanxi 710048, China.
†These authors contributed equally to the work.

stretchable sensors and wearable energy providers.[29] All these aligned PVDF fibers were mostly deposited across a pair of electrodes attaching on a flexible substrate,[24,30] which would require a large bending of the substrate to produce an adequate stretching of the fibers for an effective conversion. Some other researchers sandwiched randomly oriented electrospun PVDF nanofiber membranes[31, 32] or aligned P(VDF-TrFE) nanofiber webs[23] between two planar electrodes to build vibration-driven generators which generated an output voltage as high as several volts upon being excited mechanically by a force normal to the electrodes. However, the electric potential across the nanofiber membrane in these generators could be generated by molecular dipoles only partially aligned along the direction normal to the electrodes.[23] Furthermore, it would be a great challenge to ensure a full connectivity of these nanofibers with the upper electrode since the upper electrode was created separately. The possible sliding between the upper electrode and the piezoelectric nanofibers would result in increased wearing and contact instability[11, 33], thereby influencing the lifetime and output stability of the devices negatively.

In order to enhance the piezoelectric performance, it is highly desirable to align both the molecular dipoles and the fiber elongation of the sandwiched piezoelectric material simultaneously into a full coincidence with the normal to the planar electrodes. Furthermore, a robust contact between the piezoelectric fibers and electrodes can be also critical for output stability and efficient charge collection. Based on these two considerations, this paper presents a self-connected vertically integrated generator (or SCVIG) made of piezoelectric P(VDF-TrFE) microfiber array which has an poling orientation fully aligned to the principal exciting force for vibration energy harvesting. In our strategy, a P(VDF-TrFE) film coated on a planar electrode is firstly patterned into an array of shallow micropillars by hot embossing, and another planar electrode is then placed above the pre-formed micropillars with an air-clearance. A voltage applied across the two parallel electrodes tends to pull the thermoplastic micropillars electrohydrodynamically (EHD) upward,[34] generating a microfiber array finally in contact with the upper electrode. Such a thermoplastic and EHD deformation of the microfibers, featured simultaneously by an electric field and by a microfiber elongation dominantly vertical to the electrode throughout the process, leads to a poling orientation of P(VDF-TrFE) well aligned normal to the electrodes, therefore coincident with the principal strain for the generator excited normal to the capacitor. The adequate contact of the microfiber array with the upper electrode is detected by monitoring a current of the polymer across the electrode pair *in situ* to ensure a robust electric connectivity. Under periodic mechanical impact, electric signals are repeatedly generated from the SCVIG device and used to power a seven-segment indicator, four commercial colored (red, green, blue and yellow) light-emitting diodes (LEDs) connected in series, and a large-scale liquid-crystal display (LCD) screen.

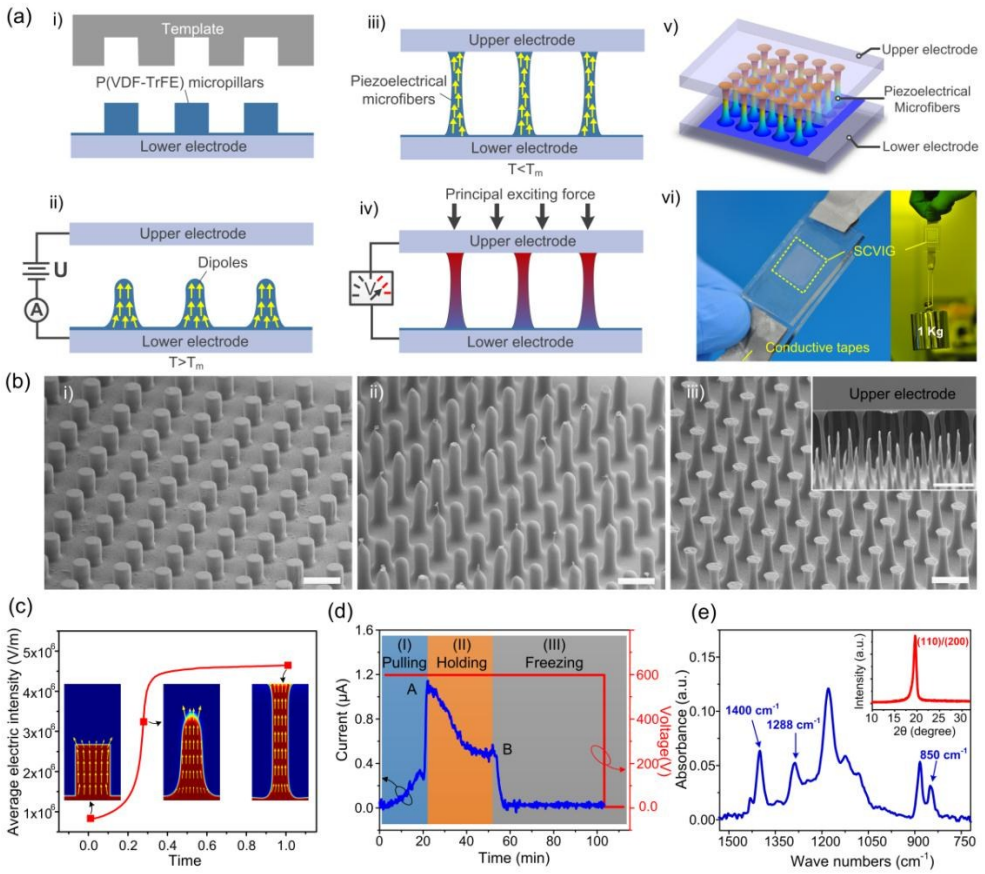

Fig.1 (a) Experimental steps for building and exciting SCVIG (i-v); (vi) shows the photograph of SCVIG sample (with the right inset showing a 1Kg weight hanging to the device). (b) SEM images of the polymer at the beginning (i), middle (ii) and ending (iii) of the micropillar deformation (with the upper electrode removed); the inset of (iii) shows the cross-section SEM image of the microfiber array that are sandwiched between the upper and lower electrodes. (c) The vectored electric field (denoted by the yellow arrows) and the average electric intensity (denoted by the red curve) inside a micropillar during its deformation. (d) Current

across capacitor devices during the EHD process which is divided into three phases, i.e. Pulling, Holding and Freezing (the thermopoling mainly happens during Pulling and Holding, while during Freezing the gradual cooling of the microfibers is accompanied by a re-crystallization of the polymer, freezing the poling orientation of the molecular dipoles so produced). (e) FTIR spectra of the microfiber array after the EHD process. The inset in (e) shows an X-ray diffraction measurement on the sample. Scale bars: 30μm

Results and discussion

Fabrication of the SCVIG by patterned EHD pulling

The fabricating process for such a generator is illustrated in Figure 1a, with some detailed information included in Experimental Section. Firstly, the P(VDF-TrFE) film coated on a planar conductive substrate (ITO for a visibility in our experiment, as the lower electrode) is patterned into a shallow micropillar array by hot embossing (Figure 1a-i). Then another planar conductor (also an ITO plate in our experiment) as the upper electrode is placed above the pre-formed micropillar array with a proper air clearance to form a capacitor-like set-up. The air clearance is adjusted by properly distributed dielectric Kapton spacers sandwiched between the two electrodes. The assembly is then thermally maintained at a temperature of 160℃, which is higher than the melting temperature of P(VDF-TrFE) (T_m=150 ℃), while a DC voltage is applied to the electrode pair. The voltage applied across the electrodes produces a non-uniform electric field on the air-polymer interface due to a spatial modulation by the pre-formed micropillars, leading to a spatially modulated Maxwell force which has a maximum vertical component on the micropillars top. Such a force tends to pull the thermoplastic micropillars upward into microfibers which bridge to the upper electrode. Because of the large air clearance, the flat polymer on the non-patterned substrate can't be pulled upward, only the micropillar array have a proper initial height can be pulled upward to get to the upper electrodes. While the micropillars undergo an axial extension during the deformation, the molecular dipoles inside the polymer can be expected to be aligned vertically due to the combined thermoplastic and EHD effect. The full contact of the microfibers with the upper electrode can be detected by spotting a peek of the current monitored across the capacitor (Figure 1a-ii), which is quite critical for producing the adequate connectivity of the electrode and polymer as required for a life-robust device. In our experiments, it takes about 30-40 minutes for the microfiber array to get to the upper electrode after the temperature arises to 160℃. When the micropillars are pulled to contact the upper electrode，Maxwell force will be balanced by the surface tension. So after a slight transverse spreading of micropillars on the upper electrode due to the electrowetting effect, the microfibers will reach to a steady state. After an annealing time of about half an hour, a slow cooling of the sample to room temperature cures the structure, inducing a re-crystallization of the P(VDF-TrFE) microfiber array at the same time. Obviously, due to the microfiber extension and dipole orientation both aligned fully along the normal to the planar electrodes, the SCVIG created by the experimental steps above (as shown in Figure 1a-iii) can be expected to produce the best piezoelectric response to an normal excitation (the principal force for this capacitor-shape generator, as shown in Figure 1a-iv). The entire SCVIG device is made of a well-bridged electrode pair sandwiching the piezoelectric P(VDF-TrFE) microfiber array, as shown in Figure 1a-v. The photograph of a SCVIG sample with an effective area of 10mm×10mm was fabricated, as shown in Figure 1a-vi. Supporting Information Figure S1 presents the snapshots for the dynamic deformation of the pre-formed and liquefied micropillar array, as obtained by a numerical simulation based on an liquid–air phase-field formulation of the EHD problem in our previous publication.[35] Figure 1b shows the SEM images obtained for the micropillars correspondingly deformed at the beginning, middle, and ending of the EHD process. The initial micropillars generated via hot embossing have a diameter of 15μm and a height of 22μm. After the EHD process at a voltage of 600V, the microfibers with a diameter of ~8μm and a height of ~50μm are generated. The inset of Figures 1b-iii provides a SEM image at a cross section of the generator, showing the mushroom shaped microfibers well connected to the electrodes (where the sharp microfibers are those broken ones caused during the removal of the cut-off upper electrode). The robust adhesion of the two electrodes to the P(VDF-TrFE) microfiber array was proved by hanging a 1-kilogram weight to one electrode while another electrode was clamped, as shown in the right inset of Figure 1a-vi.

Being different from the common poling processes[21,30,36] where usually the polymeric micro-/nano-structuring and poling were performed in separate steps, the thermoplastic elongation and thermopoling of the micro-pillars or fibers are synchronously accomplished in the proposed method. Figure 1c presents the direction of the electric field and the average electric intensity within the polymeric micropillar during the EHD process. The average electric intensity inside the microfiber increased during the EHD process and reached a maximum when the microfiber get to the upper electrode, as denoted by the red curve. It is important to note that the direction of the electric field (denoted by the yellow arrows) is always dominantly along the axis of the microfiber throughout the micropillar elongation, which ensures a molecular poling orientation of micropillars fully aligned along the axis of the finally formed microfiber. Such an oriented poling will align the molecular dipoles inside the fibers coincident with the principal excitation for maximized power conversion. So during the patterned EHD Pulling progress, the thermoplastic elongation of micropillars and the *in situ* poling of the elongated fibers are accomplished in one-step. The current across the capacitor bridged by the P(VDF-TrFE) microfibers is mainly composed of two components, i.e. the polarization current due to the dipoles orientation and the leaky current due to the minor free electrons within this typical dielectric.[37] Figure 1d shows the current experimentally monitored at a voltage of 600V during the EHD process, which is divided into three phases. The moment the microfiber array elongates into a full contact with the upper electrode, the current jumps to a peek because the current component due to the dipoles orientation reaches a maximum (shown at moment A), which, due a time-relaxation in the dipole orientation,[38] is followed by a gradual declining to a constant, the leaky current component. Obviously, the peek current can be readily spotted and used to detect the adequate contact of the microfibers with the upper electrode,[39] which is desirable for ensuring the connectivity of the generator. After the current peek is spotted, the thermopoling process is sustained (i.e. phase Holding, which lasted about half an hour in our experiment), allowing for a maximized polarization, because the average electric intensity inside the microfibers have reached a maximum during Holding,

as shown in Figure 1c by the red curve. The polymeric crystallinity of the microfiber array can characterized by Fourier Transform Infrared (FTIR) spectrum in the wave number range of 750-1500cm^{-1} (Figure 1e). The IR absorption peaks that appear at 850, 1288 and 1400 cm^{-1} bands are the evidence of the β crystalline phase.[40] A X-ray diffraction (XRD) measurement were also carried out at 2θ angles ranging from 10 ° to 30 ° to confirm the crystalline phase of microfiber array, as shown by the inset in Figure 1e, where the spectrum peak at 19.9 °, corresponding to the overlapping of (110) and (200) reflections, is attributable to the β phase.[41]

Experimental and theoretical studies of SCVIG.

In order to characterize the performance of the SCVIG, an experimental set-up was designed, as shown in Figure 2a,b. The SCVIG sample was positioned under a cylindrical probe, which was driven by an electromechanical vibrator, with some detailed information included in Experimental Section. Figure 2c,d charts the voltage and current outputs of the SCVIG excited in periodic impact by an electromechanical vibrator, which was driven by a square-pulse signal at 1 Hz and a pulse width of 0.1 sec, corresponding to a peak of 25N for the exciting force. As it can been seen from these Figures, for this SCVIG sample with an effective area of 10mm×10mm, the peak values of the output voltage and current were found to be

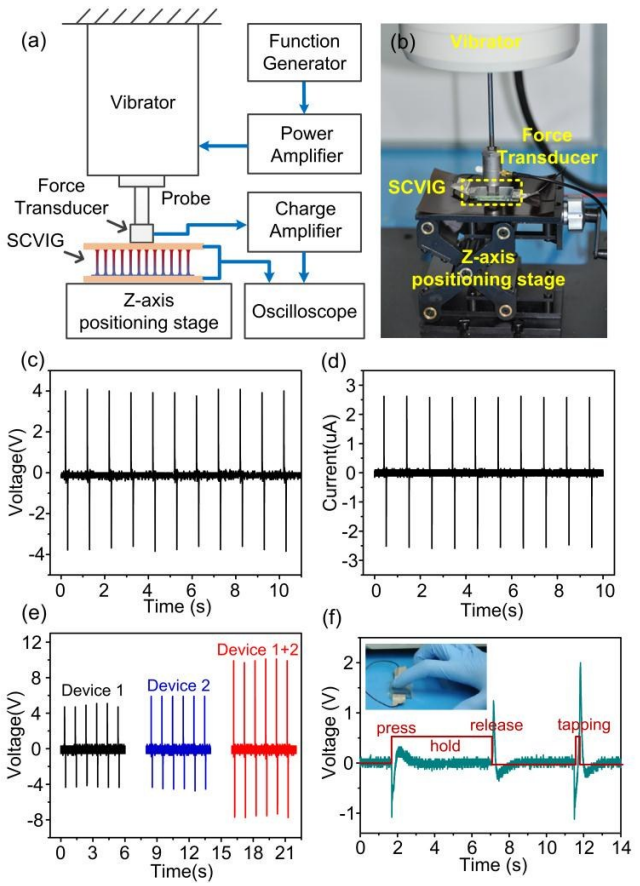

Fig.2 (a) Schematic diagram of experimental setup for the SCVIG excitation; (b) Photograph of the experimental setup; (c), (d) Measured the output voltage and current signals of the SCVIG under continuous impact, respectively. (e) The output voltage signals generated from two difference SCVIG devices connected in serial. (f) Output voltage measured using a finger to load the generator in holding and tapping modes.

4.0V for external load 10MΩ and 2.6μA for external load 50kΩ, respectively. This output performance is higher or comparable to the recently reported values for other P(VDF-TrFE) based piezoelectric devices.[8,23,42,43] To verify that the output monitored was purely generated by the SCVIG as a whole, the widely accepted polarity switching test and linear superposition test were conducted.[33] For P(VDF-TrFE) piezoelectric microfibers, upon reversing the electrode connections, a switch in the polarity of the observed signal was observed, as shown in Supporting Information Figure S2. To observe the linear superposition phenomena, two SCVIG devices were placed together under the probe of the vibrator to be impacted simultaneously during the superposition experiment (Figure S3, Supporting Information). When the two devices were serially connected, the sample output approximately added up together a voltage of nearly 10.0 V was obtained (one device generated a 4.6 V peak potential, and the other device generated a 5.8 V peak potential for the same pressure, Figure 2e). From these two verification results, the periodically measured output signals are indeed from the SCVIG device. For a comparison, an experiment of a non-piezoelectric polymethylmethacrylate (PMMA) microfiber array fabricated by the same process showed no significant electrical output, which rules out any visible contribution of the artifacts or friction to the electric output of the SCVIG device (as shown in Supporting Information Figures S4). As a concept application, we demonstrate the conversion of human finger movement into electricity as energy harvester from a key-typing. The small device was driven by a slight pressing motion of finger tapping, and showed a perfect synchronization of the finger motion with induced voltage (see Video S1 in Supporting Information). As a matter fact, during the process, a dynamic load was applied on the SCVIG in a press-hold-release mode, resulting in an output response as shown in Figure 2f. During the pressing, the mechanical strain induces piezoelectric bound charges which results in a piezoelectric potential along the microfibers. This potential will drive a flow of free electrons from the low-potential electrode to the high-potential one through an external circuit and with these free electrons accumulated at the electrode-microfiber interface to balance the piezoelectric potential, leading to a negative voltage peak. Since the piezoelectric bound charges are balanced by the free electrons from external circuitry at a constant strain (during holding), no visible voltage signal appears. When the strain is released, the positive voltage distribution is generated due to piezoelectric potential diminished and the accumulated charges moved back to the opposite electrode. This response behavior is typical of any piezoelectric P(VDF-TrFE) generators.

The effective electric power output of the SCVIG was obtained by measuring the voltage across different load resistors from 0.01MΩ to 10MΩ with applying force of 30N at 1 Hz, see Figure 3a. Figure 3b shows the instantaneous power density of the SCVIG measured across various load resistors. This bell-shaped relationship is matched well with previously analyzed results discussed by Briscoe et al.[44] The maximum measured instantaneous output power reached 5.0μW/cm^2 with a load resistance of 2.3MΩ. On the other hand, to study the frequency dependence of SCVIS's output, various cycling frequencies ranging from 1 to 100 Hz for the same applied impact force were applied by the vibrator. The response of the SCVIG to different impact frequencies is shown in Figure 3c, showing a wide frequency of mechanical impacts can be harvested by the SCVIG device. The relationship between the frequency and the peaks of the output is shown in Figure 3d.

When we increase the frequency, generated voltage of the SCVIG increases possibly because the electrons in the external circuit have a shorter time to balance the piezoelectric potential.[45] So to obtain higher instantaneous power, higher frequency excitation is desirable. The stability of the SCVIG was also examined by continually impacting and releasing motions under a peak force of 30N at high frequency (60Hz) over an extended period of time. The voltage amplitudes exhibit high stability for 1200 cycles and these do not appear to show any significant declining for another 1200 cycles after 3 hour, as shown in Figure 3e. The right inset in Figure 3e shows the magnified output at the end of the test. The P(VDF-TrFE) patterns show high stable output performance even the applied load increased to 80N (nearly the maximum output force from our vibrator) and do not show obvious degradation with time. This stable output performance can be attributed to the good flexibility of the fiber array and the self-connected integrated design which have a robust adhesion of the two electrodes with the P(VDF-TrFE) array under significant mechanical impacting.

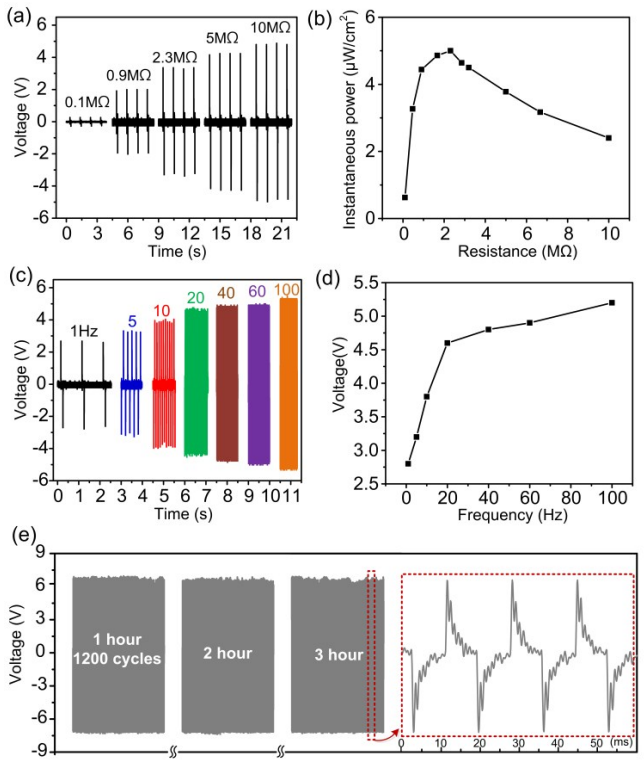

Fig.3 (a) Output voltage with various load resistors. (b) Dependence of the instantaneous power output on external load resistance, indicating maximum power output when R= 2.3MΩ. (c) Output voltage with various impact frequencies. Load resistance is 10MΩ. (d) Relationship between the peaks of the output voltage and the impact frequencies. (f) The output stability of the SCVIG operating by periodical impacting under a peak force of 30N at 60 Hz for 3 hours.

In order to demonstrate a piezoelectricity enhanced by the micro-fibering, we compared the power generation from two microfiber based SCVIGs to that from a bulk film-based generator generated using the same poling nominal electric field intensity (i.e. some voltage per unit gap of the electrode pair). The SCVIG with the microfiber array of a high aspect ratio has a diameter of ~6μm and a height of ~50μm for the fibers (Figure 4a-I), and the one of a low aspect ratio has a diameter of ~10μm and a height of ~30μm (or a Figure 4a-II). The bulk film has a thickness of 50μm and an area of 10mm×10mm for an objective comparison. The voltage output was obtained and is plotted as shown versus various changing load range from 4N to 80N in Figure 4a.The impact frequency is 1Hz. The output seems to linearly increase with the applied load and the achieved slopes of the generators with the high aspect ratio, the low aspect ratio and the bulk film are 269.4, 114.9, and 50.8 mV/N, respectively. It is important to note that the SCVIG with the high aspect ratio and with the low one can respectively produce an output of 5.4 times and 2.3 times that obtained from the bulk-film based generator. This increment ratio is higher or comparable than the previously reported nano- or microstructures array.[21,22,25] The enhanced piezoelectric output can be attributed to the improved mechanical flexibility of the microfiber array under compression.[22,25,46] The air gap between the fibers makes the array structures quite porous in nature and hence increases the stress on the piezoelectric material. Therefore, although fabrication of microfibers array reduces the volume of piezoelectric materials for generating electricity, the soft and spring-like microfibers array would yield considerably larger displacement to increase the piezoelectric potential more, a combined effect is still an increased piezoelectric output under the same external load. To verify this, finite element method (FEM) simulation is conducted using the COMSOL software package. The microfiber array can be regarded as hundreds of microfibers connected in parallel, so the piezoelectric voltage of a microfiber unit was calculated. In the simulation, because the fabricated microfibers have a pitch of 20μm, all the calculated unit blocks were modeled as 20μm×20μm which reflect actual dimensions of the fabricated devices. Figure 4b shows the geometrical configuration of the finite element method (FEM) simulation model. The lower electrode was fixed and the bottom of the P(VDF-TrFE) fiber was electrically grounded. A constant external load (50kPa) was applied to the upper electrode of the device to simplify the simulation. The detailed simulation process is described in the Supporting Information S5. Figure 4c show the simulated piezoelectric potential at the top of three P(VDF-TrFE) unit blocks. The potential of unit microfiber (I) device is in the range from 0 to 5.2871V, the potential of unit microfiber (II) device varies from 0 to 1.561V, and the peak piezoelectric potential of the flat film unit has a minimum value 0.5042V. The voltage drop across the device can be calculated by the ratio of the charge generated by the microfiber over the total capacitance which is the sum of the capacitance of the microfiber and the air gap.[46] Detailed calculation process is described in the Supporting Information S6. The calculated results of the voltage drop across the three unit devices are shown in Figure 4d. The voltage drops across the microfibers are much higher than that of the bulk film, which is in agreement with our experimental results. This experimental observations and simulation results can also be verified by the analytic solution from Dapino *et al.*[46] According to their conclusion, under the same external load, the piezoelectric voltage of the micropillar array relative to that of solid bulk PVDF film can be simplified as:

$$k = \frac{\varepsilon_r (1+s/d)^2}{\pi/4 \cdot (\varepsilon_r - 1) + (1+s/d)^2}$$

where ε_r is permittivity of P(VDF-TrFE), d is the diameter of the micropillar, s is the gap between pillars. For the P(VDF-TrFE) microfibers with the high aspect ratio in our experiment, $\varepsilon_r = 18$,[47] s=14μm, d=6μm, so that $k \approx 8.17$ which is in

agreement with our experimental observations and simulation results. Besides, the geometrical strain confinement along an axis in P(VDF-TrFE) fibers can also lead to an enhancement of the piezoelectric potential.[21,48,49] By reducing the fiber diameter under vertical stress, the stress can be geometrically more confined in the axial direction, which leads to an increased piezoelectric potential.[21] Including the fiber diameter, ratio of the gap between fibers and the aspect ratio are also able to influence piezoelectric output of the fiber array,[46] so a coupled mechanical and piezoelectric analysis of the fiber array will be further studied in the near future to optimize the size, layout, spacing, and density of the self-connected fibers in the SCVIG to enhance the piezoelectric output.

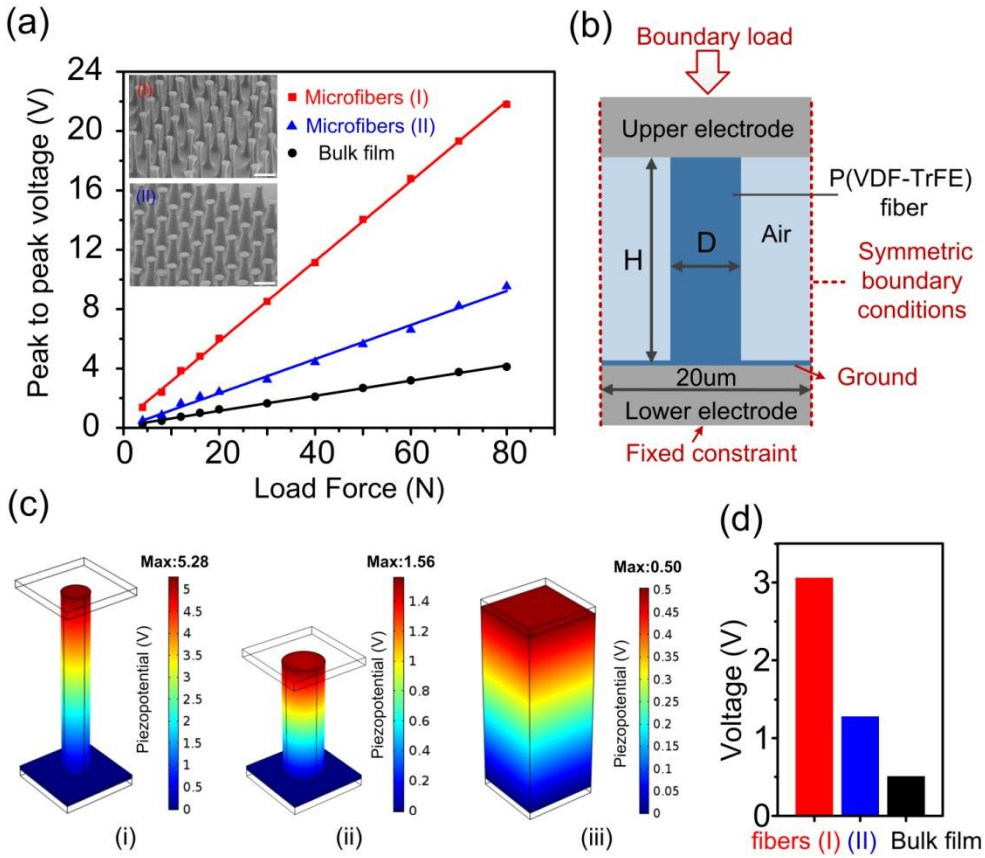

Fig.4 (a) A comparison of output voltages for SCVIG based on microfibers with two aspect ratios and for a capacitor sandwiching a bulk P(VDF-TrFE) film (black line); the inset shows SEM images for the microfibers with two aspect ratios. Scale bars: 20μm. (b) The geometrical configuration of the FEM simulation model. (c) Magnitude of simulated peak piezoelectric potential of three unit blocks. (c-i) represents the unit microfiber (I) device with a diameter of 6μm and a height of 50μm. (c-ii) represents the unit microfiber (II) device with a diameter of 10μm and a height of 30μm. (c-iii) represents a flat film unit. (d) The calculated voltage drops across three units of devices. The red, blue, and back column represents the unit microfiber (I) device, the unit microfiber (II) device and the bulk film device, respectively.

Additional energy harvesting applications

For a potential utilization of the energy harvesting technology, we demonstrated three applications of the SCVIG device to power commercial electronic devices. First, the generated electric source was successfully used to light a commercial seven-segment indicator with the electricity generated from the SCVIG device. To convert the alternating voltage outputs to direct signals, the SCVIG device was incorporated into a predesigned circuit (Figure 5a) and the rectified voltage output reached 8.6V (see the inset in Figure 5b). Figure 5b shows the voltage-charging time relationship of a 47μF capacitor, where the voltage can be charged to about 5.1 V under 60 Hz repeated compressive impacts for 270s. It can be used to drive the commercial seven-segment indicators, as shown in Figure 5c-i (see Supporting Information Video S2). The letters "NTRC" are the acronym of our research group (Nanotechnology Research Center). Figure 5c-iii shows the second application which the red (R), green (G), blue (B) and yellow (Y) LEDs aligned in serial are successfully operated by connecting the three charged capacitors in series (see Supporting Information Video S3). Figure 5c-ii shows the total usable energy was about 14.6 V after connecting the three charged capacitors in series which is higher than the turn-on voltage ≈10V of RGBY LED arrays. In the third application, a 4-bit liquid crystal display (LCD) screen was directly lighted by output signals without the energy storage process (Figure 5d). More details are shown in video 4 in the Supporting Information. Figure S7 in the Supporting Information presents the output voltage measured from the SCVIG device at an impacting frequency of 1 Hz, which was used to drive the LCD screen.

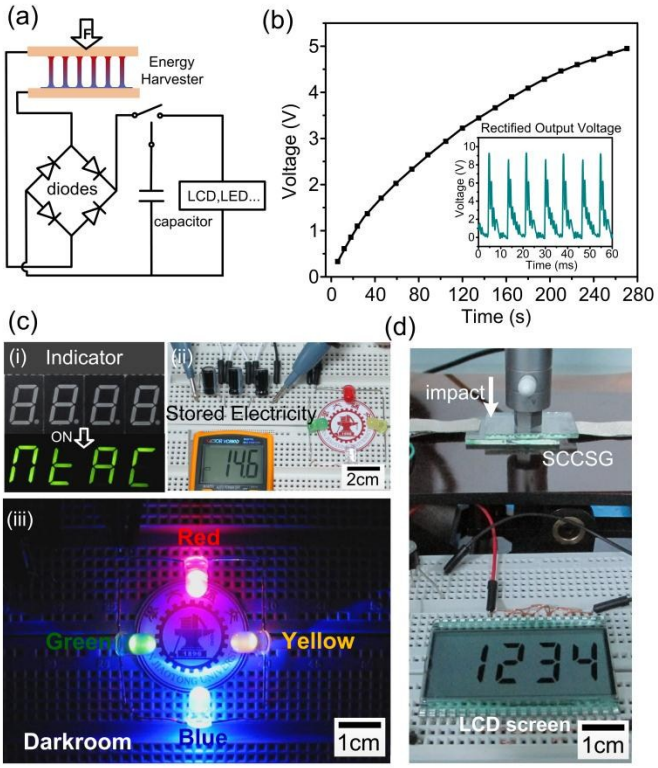

Fig. 5 (a) Circuit for rectifying, charging capacitors and lighting electronic devices. (b) Voltage-charging time relationship of a 47μF capacitor by using the SCVIG device, the inset in (b) shows the measured output voltage after rectification. (c) A seven-segment indicator driven by the SCVIG device (left, i); the measured voltage (~14.6V) when three 47μF capacitors are aligned in a serial (right, ii); A captured photograph of the RGBY color LEDs lit by the power source generated from a SCVIG device (bottom, iii). (d) A 4-bit LCD screen operated by electricity generated during impacting/releasing motions of a SCVIG device without external circuits.

Conclusions

In conclusion, we demonstrated a self-connected vertically integrated generator (SCVIG) made of piezoelectric P(VDF-TrFE) microfiber array by patterned electrohydrodynamic pulling. The electric field applied between the electrode pair sandwiching the initial micropillar array pulls the microfibers into a final contact with the upper electrode while at the same time aligning the molecular dipoles and the piezoelectric fibers synchronously into a full coincidence with the normal pressure applied to the planar electrodes. An adequate contact of the microfibers with the electrodes can well be detected by monitoring the current across the electrode pair during the EHD process *in situ* for a robust electric connectivity. So the resultant piezoelectric microfiber array structure sandwiched between a well-bridged electrode pair possesses the advantage of efficient charge collection and output stability due to intimate contact between the microfibers and electrodes. Besides, the microfiber array structure of the piezoelectric materials makes it quite spring-like in nature and hence relatively easy to compress, leading to enhanced energy adsorption capacity under compression. Finally, the electrical power generated from the piezoelectric device is used to operate a seven-segment indicator, four commercial colored (red, green, blue and yellow) light-emitting diodes (LEDs) connected in series, and a large-scale liquidcrystal display (LCD) screen. Due to the effective fabrication method, high energy generation and good mechanical durability, the power generator is highly attractive to self-powered electronic devices for either energy-harvesting or sensing purposes.

Experimental Section

Generation of the Shallow Micropillar Array. P(VDF-TrFE) powder with a molar ratio of 70/30 (purchased from Kunshan Hisense Electronics Co.,Ltd) was dissolved in dimethylformamide solution (10wt%) and spin coated onto an ITO (indium tin oxide)-deposited substrate (an ITO coated glass for a visibility in our experiment) to produce 5-6 μm thick film. The as-prepared sample was then heated on a hot plate at 140℃ for 3 min to evaporate the residual solvent. During hot embossing, a PDMS mold arrayed with microcavities is pressed against the P(VDF-TrFE) film under a pressure of 4.8 MPa at 160 ℃ for 30 min. After de-molding, a P(VDF-TrFE) micropillar array was generated on the conductive ITO substrate (functioning as the lower electrode).

The experimental setup for the SCVIG excitation. The SCVIG sample was positioned under a cylindrical probe, which was driven by an electromechanical vibrator (SINOCERA JZK-10). The exciting signal from a function generator (Agilent 33220A) is amplified by a power amplifier (SINOCERA YE5871A) to drive the vibrator. The magnitude of the force input to the SCVIG sample was measured by a calibrated piezoelectric force transducer (SINOCERA CL-YD-331) having a sensitivity of 3.37 pC/N, which was placed between the probe and the upper electrode. The output from the force transducer was passed through a charge amplifier (ECON MI-2004-2) before being recorded on a oscilloscope (Tektronix DPO3034). The electrical output signal from the SCVIG samples was also recorded by the Tektronix DPO3034 oscilloscope. The output voltage was measured with a 10 MΩ probe and the output current was measured using a 100 kΩ external resistance.

Measurement and Characterization. The DC voltage used in the thermopoling and EHD process was applied by an amplifier/controller (TREK 610E H.V.). The current across SCVIG sample is *in situ* monitored using an oscilloscope (Tektronix DPO3034). All the SEM images were captured using a HITACHI SU8010 SEM instrument. Wide-angle X-ray diffraction patterns were collected on a SmartLab X-ray diffraction system with Cu-Kα radiation at λ = 1.5418 Å. The Fourier transform infrared absorption spectroscopy (FTIR) was carried out with a Bruker VERTEX 70.

Acknowledgements
This work is financed by the NSFC Major Research Plan on Nanomanufacturing (grant no. 91323303), and NSFC Funds (grant no. 51305347 and 51275401).

Notes and references

[a]Micro- and Nano-technology Research Center, State Key Laboratory for Manufacturing Systems Engineering, Xi'an Jiaotong University, Xi'an, Shaanxi 710049, China
[b]College of Printing and Packaging Engineering, Xi'an University of Technology, Xi'an, Shaanxi 710048, China
*Corresponding authors: jyshao@mail.xjtu.edu.cn (Jinyou Shao)

1 M. Lee, C. Y. Chen, S. Wang, S. N. Cha, Y. J. Park, J. M. Kim, L. J. Chou and Z. L. Wang, *ACS nano*, 2012, **24**, 1759-1764.
2 K. H. Kim, K. Y. Lee, J. S. Seo, B. Kumar and S. W. Kim, *Small*, 2011, **7**, 2577-2580.
3 C. K. Jeong, K.-I. Park, J. H. Son, G.-T. Hwang, S. H. Lee, D. Y. Park, H. E. Lee, H. K. Lee, M. Byun and K. J. Lee, *Energy Environ. Sci.*, 2014.
4 Z. L. Wang and J. Song, *Science*, 2006, **312**, 242-246.
5 J. Chang, M. Dommer, C. Chang and L. Lin, *Nano Energy*, 2012, **1**, 356-371.
6 Y. Qin, X. Wang and Z. L. Wang, *Nature*, 2008, **451**, 809-813.
7 C. Sun, J. Shi, D. J. Bayerl and X. Wang, *Energy Environ. Sci.*, 2011, **4**, 4508-4512.
8 L. Persano, C. Dagdeviren, Y. Su, Y. Zhang, S. Girardo, D. Pisignano, Y. Huang and J. A. Rogers, *Nat. Commun.*, 2013, **4**, 1633.
9 X. Chen, S. Xu, N. Yao and Y. Shi, *Nano Lett.*, 2010, **10**, 2133-2137.
10 C. Dagdeviren, B. D. Yang, Y. Su, P. L. Tran, P. Joe, E. Anderson, J. Xia, V. Doraiswamy, B. Dehdashti and X. Feng, *Proc. Natl. Acad. Sci.*, 2014, **111**, 1927-1932.
11 S. Xu, Y. Qin, C. Xu, Y. Wei, R. Yang and Z. L. Wang, *Nat. Nanotechnol.*, 2010, **5**, 366-373.
12 Y. Yang, H. Zhang, G. Zhu, S. Lee, Z.-H. Lin and Z. L. Wang, *ACS nano*, 2012, **7**, 785-790.
13 G. T. Hwang, H. Park, J. H. Lee, S. Oh, K. I. Park, M. Byun, H. Park, G. Ahn, C. K. Jeong and K. No, *Adv. Mater.*, 2014, **26**, 4880-4887.
14 S. Xu, Y.-w. Yeh, G. Poirier, M. C. McAlpine, R. A. Register and N. Yao, *Nano Lett.*, 2013, **13**, 2393-2398.
15 S.-H. Shin, Y.-H. Kim, M. H. Lee, J.-Y. Jung and J. Nah, *ACS nano*, 2014, **8**, 2766-2773.
16 K. I. Park, M. Lee, Y. Liu, S. Moon, G. T. Hwang, G. Zhu, J. E. Kim, S. O. Kim, D. K. Kim and Z. L. Wang, *Adv. Mater.*, 2012, **24**, 2999-3004.
17 S. Lee, R. Hinchet, Y. Lee, Y. Yang, Z. H. Lin, G. Ardila, L. Montès, M. Mouis and Z. L. Wang, *Adv. Funct. Mater.*, 2014, **24**, 1163-1168.
18 L. Lin, Y. Hu, C. Xu, Y. Zhang, R. Zhang, X. Wen and Z. Lin Wang, *Nano Energy*, 2013, **2**, 75-81.
19 K. I. Park, C. K. Jeong, J. Ryu, G. T. Hwang and K. J. Lee, *Adv. Energy Mater.*, 2013, **3**, 1539-1544.
20 A. Holmes-Siedle, P. Wilson and A. Verrall, *Mater. Des.*, 1984, **4**, 910-918.
21 S. Cha, S. M. Kim, H. Kim, J. Ku, J. I. Sohn, Y. J. Park, B. G. Song, M. H. Jung, E. K. Lee and B. L. Choi, *Nano Lett.*, 2011, **11**, 5142-5147.
22 Y. Mao, P. Zhao, G. McConohy, H. Yang, Y. Tong and X. Wang, *Adv. Energy Mater*, 2014, **4**, 1301624.
23 D. Mandal, S. Yoon and K. J. Kim, *Macromol. Rapid Commun.*, 2011, **32**, 831-837.
24 C. Chang, V. H. Tran, J. Wang, Y.-K. Fuh and L. Lin, *Nano Lett.*, 2010, **10**, 726-731.
25 N. Soin, T. H. Shah, S. C. Anand, J. Geng, W. Pornwannachai, P. Mandal, D. Reid, S. Sharma, R. L. Hadimani and D. V. Bayramol, *Energy Environ. Sci.*, 2014, **7**, 1670-1679.
26 V. Bhavanasi, D. Y. Kusuma and P. S. Lee, *Adv. Energy Mater.*, 2014, 4.
27. Y. Ding, Y. Duan and Y. Huang, *Energy Technol.*, 2015, 3, 1-9.
28. Y. Duan, Y. Huang, Z. Yin, N. Bu and W. Dong, *Nanoscale*, 2014, 6, 3289-3295.
29. Y. Huang, Y. Duan, Y. Ding, N. Bu, Y. Pan, N. Lu and Z. Yin, *Sci. Rep.*, 2014, 4.
30 B. J. Hansen, Y. Liu, R. Yang and Z. L. Wang, *ACS nano*, 2010, **4**, 3647-3652.
31 J. Fang, H. Niu, H. Wang, X. Wang and T. Lin, *Energy Environ. Sci.*, 2013, **6**, 2196-2202.
32 J. Fang, X. Wang and T. Lin, *J. Mater. Chem.*, 2011, **21**, 11088-11091.
33 R. Yang, Y. Qin, L. Dai and Z. L. Wang, *Nat. Nanotechnol.*, 2008, **4**, 34-39.
34 E. Schäffer, T. Thurn-Albrecht, T. P. Russell and U. Steiner, *Nature*, 2000, **403**, 874-877.
35 H. Tian, J. Shao, Y. Ding, X. Li and X. Li, *Electrophoresis*, 2011, **32**, 2245-2252.
36 C. Li, P.-M. Wu, S. Lee, A. Gorton, M. J. Schulz and C. H. Ahn, *J. Microelectromech. Syst*, 2008, **17**, 334-341.
37 W. Urbaniak-Domagala, *J. Electrost.*, 2013, **71**, 456-461.
38 K. Zimmerman, F. Ghebremichael, M. Kuzyk and C. Dirk, *J. Appl. Phys.*, 1994, **75**, 1267-1285.
39 P. Goldberg‐Oppenheimer and U. Steiner, *Small*, 2010, **6**, 1248-1254.
40 N. M. Reynolds, K. J. Kim, C. Chang and S. L. Hsu, *Macromolecules*, 1989, **22**, 1092-1100.
41 K. Lau, Y. Liu, H. Chen and R. Withers, *Adv. Condens. Matter Phys.*, 2013, 2013.
42 S. H. Bae, O. Kahya, B. K. Sharma, J. Kwon, H. J. Cho, B. Ozyilmaz and J. H. Ahn, *ACS nano*, 2013, **7**, 3130-3138.
43 J. H. Lee, K. Y. Lee, M. K. Gupta, T. Y. Kim, D. Y. Lee, J. Oh, C. Ryu, W. J. Yoo, C. Y. Kang and S. J. Yoon, *Adv. Mater.*, 2014, **26**, 765-769.
44 J. Briscoe, N. Jalali, P. Woolliams, M. Stewart, P. M. Weaver, M. Cain and S. Dunn, *Energy Environ. Sci.*, 2013, **6**, 3035-3045.
45 L. Gu, N. Cui, L. Cheng, Q. Xu, S. Bai, M. Yuan, W. Wu, J. Liu, Y. Zhao and F. Ma, *Nano Lett.*, 2012, **13**, 91-94.
46 J. Xu, M. Dapino, D. Gallego-Perez and D. Hansford, *Sens. Actuators, A*, 2009, **153**, 24-32.
47 P. Martins, A. C. Lopes and S. Lanceros-Mendez, *Prog Polym Sci*, 2014, **39**, 683-706.
48 W. Wu, S. Bai, M. Yuan, Y. Qin, Z. L. Wang and T. Jing, *ACS nano*, 2012, **6**, 6231-6235.
49 S. M. Kim, J. I. Sohn, H. J. Kim, J. Ku, Y. J. Park, S. N. Cha and J. M. Kim, *Appl. Phys. Lett.*, 2012, **101**, 013104.
50 M.-L. Seol, H. Im, D.-I. Moon, J.-H. Woo, D. Kim, S.-J. Choi and Y.-K. Choi, *ACS nano*, 2013, **7**, 10773-10779.